Supplementary information

Two-dimensional materials saturable absorbers: Towards compact visible-wavelength all-fiber pulsed lasers

Zhengqian Luo[a†], Duanduan Wu[a†], Bin Xu[a], Huiying Xu[a], Zhiping Cai[a★], Jian Peng[b], Jian Weng[b★], Shuo Xu[c], Chunhui Zhu[c], Fengqiu Wang[c★], Zhipei Sun[d], Han Zhang[e]

[a]Department of Electronic Engineering, Xiamen University, Xiamen 361005, China

[b]Department of Biomaterials, College of Materials, Xiamen University, Xiamen 361005, China

[c]School of Electronic Science and Engineering, Nanjing University, Nanjing 210023, China

[d]Department of Micro- and Nanosciences, Aalto University, FI-02150 Espoo, Finland

[e]College of Optoelectronic Engineering, Shenzhen University, Shenzhen 518060, China

[†]These authors contributed equally to this work.

★e-mail: zpcai@xmu.edu.cn, jweng@xmu.edu.cn, fwang@nju.edu.cn

Chemicals and apparatus. MoS_2 (Product Number 41827), WS_2 (Product Number 11829) and $MoSe_2$ (Product Number 13112) powders were purchased from Alfa Aesar. NMP, dimethyl formamide (DMF) and lysine were purchased from Green Bird Science and Technology Development (Xiamen, China). All other reagents were of analytical reagent grade, and used as received. Doubly distilled water was used in all the processes of aqueous solution preparation and washing.

Characterization. The micrographs of samples were taken using a TEM (JEOL JEM-2100) with the accelerating voltage of 200 kV. The samples were prepared by placing 20 μL of the colloidal solutions on copper grids coating with lacey carbon film for TEM and were allowed to dry in air. AFM images were acquired in tapping mode in air using a Digital Instrument Nanoscope®. The samples were prepared by placing 20 μL of 10−fold diluted solutions onto the freshly cleaved mica for 5 min, gently rinsed

with deionized water, and dried in vacuum overnight. XRD (Philips PANalytical X'Pert) equipped with Cu Ka radiation (λ = 1.542 Å) over the 2θ range of 10–80° was used to characterize the structure of TMDs. Sample was prepared by depositing a film on the surface of glass slide. The ultraviolet-visible (UV–vis) absorption spectra were measured on UV–vis spectrometer (TU−1901), equipped with 1 cm quartz cells. The spectra were recorded in the wavelength range of 200–800 nm, at a scan speed of 400 nm min^{-1}. Raman spectra (XploRA，Jobin−Yvon) were recorded with a solid−state laser at the excitation wavelength of 532 nm.

Preparation of few-layer MoS_2: The purchased MoS_2 (200 mg) was added into DMF (200 mL) and sonicated for 20 h (KQ−250 DB) to produce the few-layer MoS_2 suspension. Few-layer MoS_2 suspension was centrifuged for 30 min at 2000 rpm to remove bulk MoS_2. Subsequently, the supernatant was decanted to another centrifuge tube. After centrifuging the supernatant at 13000 rpm for 30 min, the as-obtained product was collected into vials and dispersed in the polyving akohol (PVA) for further application.

Purchased bulk MoS_2 was characterized by XRD (Fig. S1c). All the labeled peaks can be readily indexed to rhombohedral MoS_2 (JCPDS no. 06-0097). TheTEM image (Fig. S1a) of exfoliated MoS_2 showed that the as-obtained few-layer MoS_2 was extremely thin 2D flake. Furthermore, the distances between the adjacent hexagonal lattice fringes investigated by HRTEM were 0.205 nm and 0.62 nm for MoS_2 (Fig. S1b), which was consistent with the lattice spaces of the (110) plane and (002) plane. The XRD pattern (Fig. S1c) of few-layer MoS_2 showed a high [002] orientation and some characteristic peaks disappeared compared to bulk MoS_2, which indicated that bulk MoS_2 had been successfully exfoliated. As shown in Fig. S1d, Raman spectroscopy, a powerful nondestructive characterization tool, was also used to estimate the thickness of few-layer MoS_2. The two characteristic peaks at 380 and 410 cm^{-1} are assigned to E^1_{2g} and A_{1g} modes of the bulk MoS_2. Compared with the bulk MoS_2, few-layer MoS_2 sample shows an obvious red shift of E^1_{2g} peak and blue shift of A_{1g} peak, indicating that the MoS_2 was successfully exfoliated with a thickness of

1-4 layers [s1]. Furthermore, the thickness of the as-prepared few-layer MoS_2 was characterized by AFM, as shown in Fig. S1e. The average thickness from the height profile (Fig.S1e insert) was measured to be ~2-3 nm. This result indicates that the MoS_2 nanosheets are around 3-4 layers, because the thickness of single-layer MoS_2 is 0.65 nm [s2]. Fig. S1f shows the absorption spectra of the few-layer MoS_2 dispersion, which is close to that expected [s3].

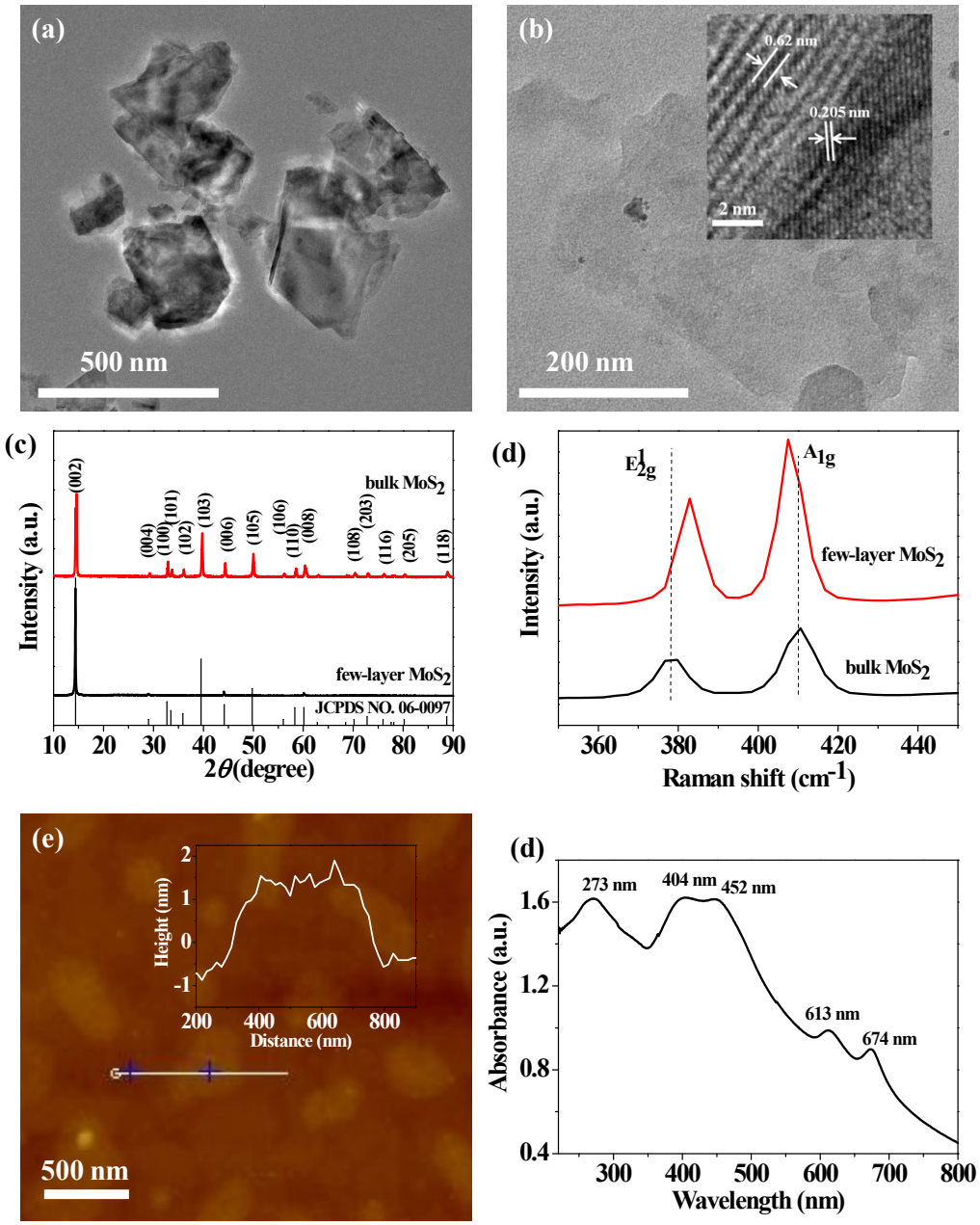

Fig. S1. (a) TEM image of few-layer MoS_2. (b) HRTEM image of few-layer MoS_2. (c) XRD patterns of bulk MoS_2 and few-layer MoS_2. (d) Raman spectra of bulk MoS_2 and few-layer MoS_2. (e) AFM image of few-layer MoS_2. Insert: corresponding height profile of few-layer MoS_2. (f) UV-vis absorption spectrum of the few-layer MoS_2.

Preparation of few-layer $MoSe_2$: The purchased $MoSe_2$ (200 mg) was added into the 1 mg mL^{-1} lysine solution (200 mL) and sonicated for 20 h (KQ−250 DB) to produce the few-layer $MoSe_2$ suspension. Few-layer $MoSe_2$ suspension was centrifuged for 30 min at 1000 rpm to remove bulk $MoSe_2$. Subsequently, the supernatant was decanted to another centrifuge tube. After centrifuging the supernatant at 13000 rpm for 30 min to remove free lysine, the as-obtained product was collected into phials and dispersed in the polyving akohol (PVA) for further application.

Bulk $MoSe_2$ was characterized by XRD (Fig. S2c). All the labeled peaks can be readily indexed to rhombohedral $MoSe_2$ (JCPDS no. 29-0914). The TEM image (Fig. S2a) of exfoliated $MoSe_2$ showed that the as-obtained few-layer $MoSe_2$ was extremely thin 2D flake. Furthermore, the distance between the adjacent hexagonal lattice fringes investigated by HRTEM was 0.28 nm for $MoSe_2$ (Fig. S2b), which was consistent with the lattice space of the (10-10) plane. The XRD pattern (Fig. S2c) of few-layer MoS_2 showed the existence of high [002] orientation and some characteristic peaks disappeared compared to bulk $MoSe_2$, which indicated that bulk $MoSe_2$ had been successfully exfoliated. As shown in Fig.S2d, the A^1_g Raman mode of the few-layer $MoSe_2$ was red-shifted slightly, also confirming that the few-layer structure of the as-prepared $MoSe_2$ [s4]. Furthermore, the thickness of the as-prepared few-layer $MoSe_2$ was characterized by AFM (Fig. S2e). The average thickness from the height profile (Fig.S2e insert) was measured to be ~2-4 nm. This result indicates that the few-layer $MoSe_2$ is around 3-6 layers, because the thickness of single-layer $MoSe_2$ is about 0.65 nm [s5]. Fig. S2f shows the absorption spectrum of the few-layer $MoSe_2$ dispersion, which is close to that expected [s3].

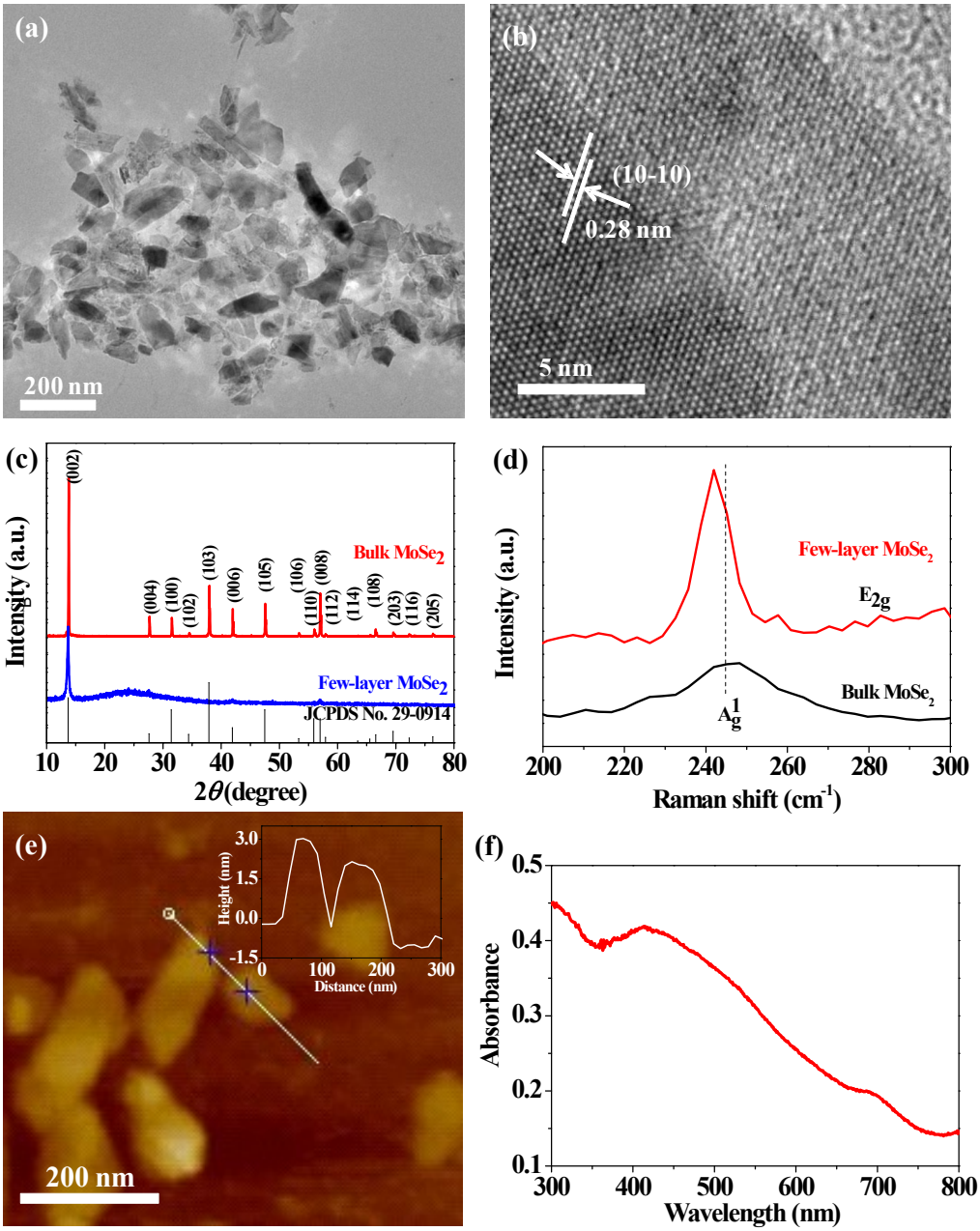

Fig. S2. (a) TEM image of few-layer $MoSe_2$. (b) HRTEM image of few-layer $MoSe_2$. (c) XRD patterns of bulk $MoSe_2$ and few-layer $MoSe_2$. (d) Raman spectra of bulk $MoSe_2$ and few-layer $MoSe_2$. (e) AFM image of few-layer $MoSe_2$. Insert: corresponding height profile of the few-layer $MoSe_2$. (f) UV-vis spectrum absorption of the few-layer $MoSe_2$.

OA Z-scan measurement of the few-layer WS_2 at 530 nm: We have experimentally performed the Z-scan measurement of the few-layer WS_2 at a green wavelength of 530 nm. As can be seen in Fig.S3, the few-layer WS_2 also shows the strong saturable absorption at 530 nm. The modulation depth can be as high as ~13%. Therefore, we believe that such 2D TMDs-based SAs could be available for green-wavelength passively Q-swithed or mode-locked laser too. In addition, because the few-layer WS_2 sample has the strong linear absorption in the blue-wavelength region, we did not perform the corresponding Z-scan measurement at blue wavelength.

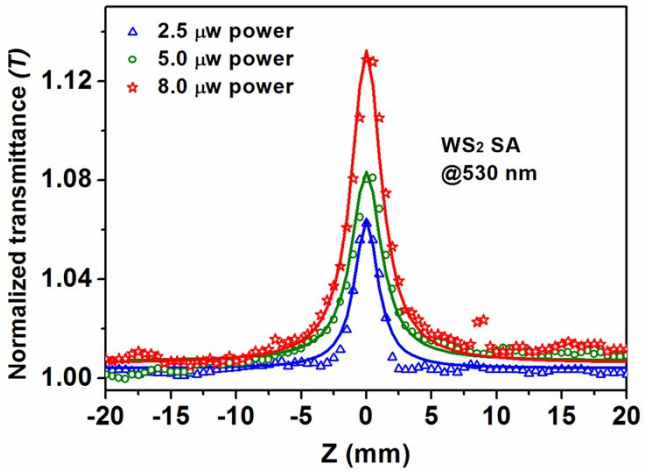

Fig. S3. OA Z-scan traces with the excitation wavelength of 530 nm and the excitation powers of 2.5, 5.0 and 8.0 μW, respectively.

Emission spectrum of the Pr^{3+}-doped ZBLAN fiber: As shown in Fig. S4, we measured the emission spectrum of the used Pr^{3+}-doped fiber excited by a 445 nm laser diode. In the reflective waveband (580~710 nm) of the cavity mirror M1 used in our experiment, there are a few of emission peaks at 609.3, 635.2 and 716.5 nm, respectively. However, it should be noted that the 635.2 nm emission peak with a spectral bandwidth of ~7 nm is highest, indicating that the optical gain of the Pr^{3+}-doped fiber around 635.2 nm is strongest. Although other emission peaks of 609.3 and 716.5 nm are also covered by the cavity mirror M1, the gain competition in the Pr^{3+}-doped fiber finally leads to the ~635 nm lasing only.

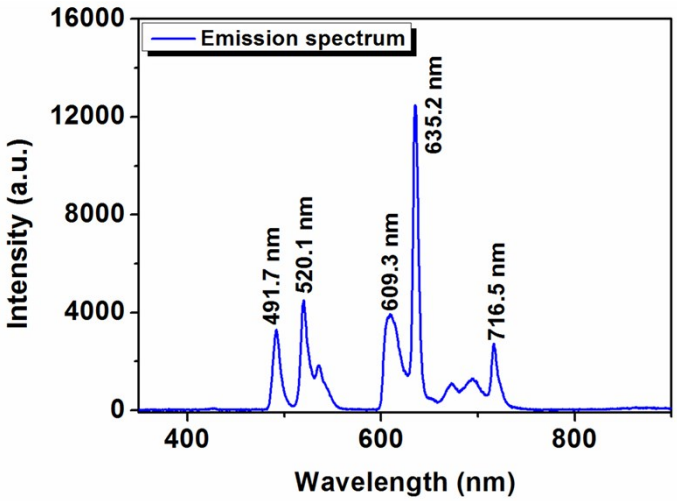

Fig.S4 The emission spectrum of the Pr^{3+}-doped ZBLAN fiber excited by a 445 nm LD.

The experimental results of MoS_2 passively Q-switched fiber laser at 635.5 nm.

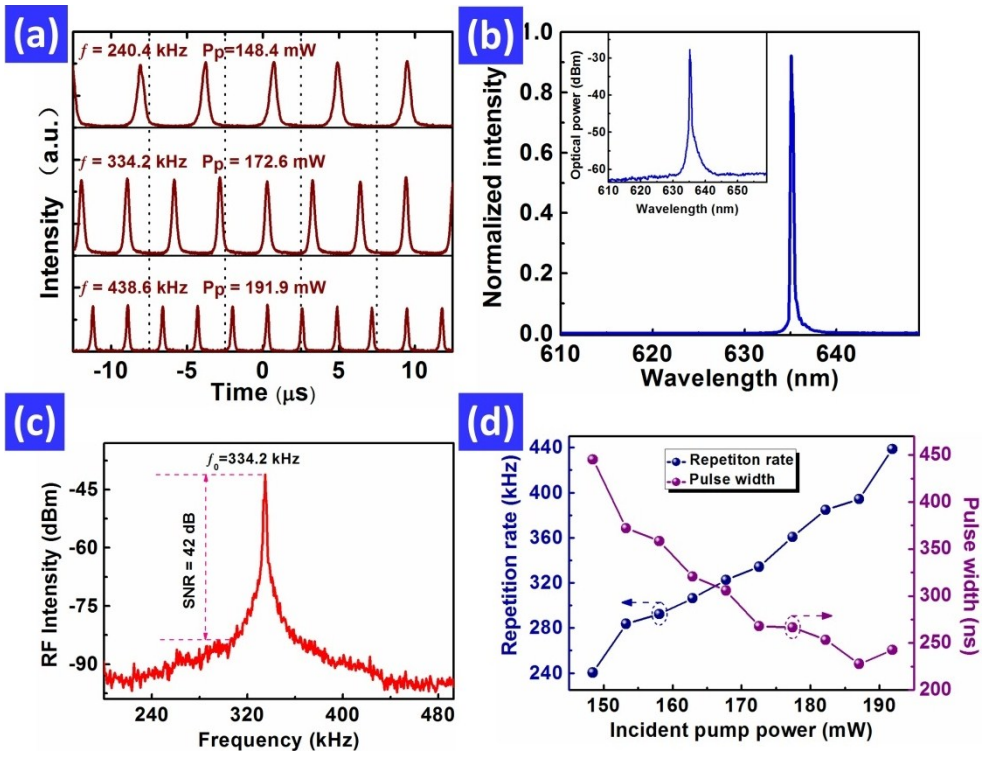

Figure S5 | The output performance of MoS_2 passively Q-switched red fiber laser. (a), The Q-switched pulse trains under the incident pump powers of 148.4 mW, 172.6 mW and 191.9 mW, respectively. (**b**), Output optical spectrum at the center wavelength of 635.1 nm. (**c**), RF output spectrum at the fundamental frequency of 334.2 kHz. (**d**), The pulse repetition rate and the pulse duration as a function of incident pump power.

With MoS_2 SA, continuous-wave (CW) operation occurred at an incident pump power of 121.9 mW, and Q-switched operation started at the incident pump power of 148.4 mW. Figure S5(a) show the typical oscilloscope traces of the Q-switched pulse trains under the pump power of 148.42, 172.6 and 191.9 mW. From Fig. S5(b), the lasing wavelength locates at 635.5 nm. As shown in Fig. S5(c), the signal-to-noise ratio (SNR) of fundamental frequency at 334.2 kHz is ~42 dB, indicating that the Q-switching operation is stable. By varying the pump power from 148.4 to 191.8 mW, the pulse repetition rate can be widely tuned from 240.4 to 438.6 kHz and the pulse duration becomes shorter and shorter with the narrowest of 227 ns, as shown in Fig. S5(d).

The experimental results of $MoSe_2$ passively Q-switched fiber laser at 635.4 nm.

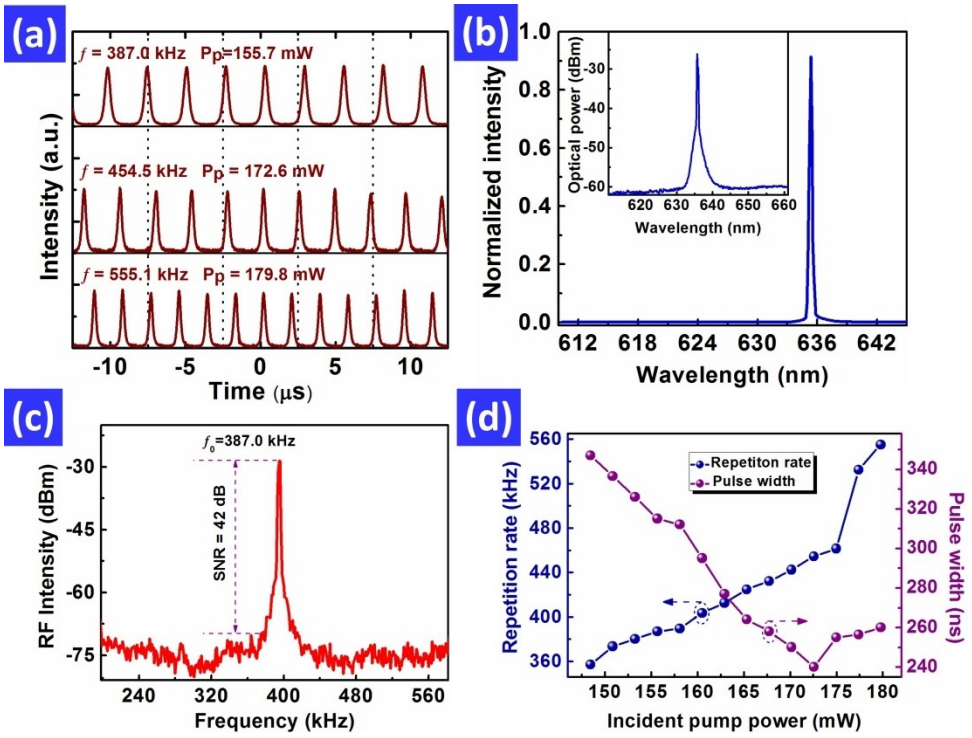

Figure S6 |The output performance of $MoSe_2$ passively Q-switched red fiber laser. (a), The Q-switched pulse trains under the incident pump powers of 155.7 mW, 172.6 mW and 179.8 mW, respectively. (**b)**, Output optical spectrum at the center wavelength of 635.4 nm. (**c**), RF output spectrum at the fundamental frequency of 387.0 kHz. (**d)**, The pulse repetition rate and the pulse duration as a function of incident pump power.

The $MoSe_2$ SA-based Q-switched red fiber laser was also achieved and measured. The CW laser threshold is 105.7 mW and the Q-switched operation occurred at the incident pump power of 146.8 mW. The typical Q-switched pulse trains with repetition rate of 387.0, 454.6 and 555.1 kHz are shown in Fig. S6(a). The center wavelength of the red laser is 635.4 nm from Fig. S6(b). The red Q-switched pulse train is stable, just as shown in Fig. S6(c), the SNR of fundamental frequency at 387.0 kHz is ~42 dB. By changing the incident pump power from 146.8 to 179.8 mW, the pulse repetition rate gradually increases from 357.1 to 555.1 kHz, and the pulse duration almost decreases linearly to the narrowest of 240 ns, as shown in Fig. S6(d).

Plasma sputter deposition system (SCT-S500):

The fiber pigtail mirror with the high-reflectivity at 635 nm was coated by Remote plasma sputtering method. The plasma sputter thin-film deposition system (SCT-S500) from the System Control Technology Inc. was used in our experiment, and the system's structure is shown in Fig. S7. An RF coil antenna surrounding a quartz tube is attached to the vacuum chamber as a side arm. The plasma is initiated and amplified by a DC launch electromagnet towards the plasma source exit. By altering the current applied to the electromagnet and in particular to the steering electromagnet, the position of the plasma beam can be adjusted to ensure good beam impingement on the target surface. To achieve a high deposition rate in reactive process, the RF power was adjusted from 1-2.2 kW and the target negative bias voltage was set from 300V-700 V respectively. During the deposition process, the system was pumped using cryo-pump with a base pressure of 6×10^{-6} Torr. Pure Argon gas was introduced to the chamber by placing a diffusion ring close to the target, and the oxygen was fed into the chamber though another diffusion ring placed as close as possible to the substrate. The oxygen flow was regulated from 0-30 sccm, the argon flow was fixed at 85 sccm, and the background pressure is approximately 5×10^{-3} Torr level. The fiber-pigtails were used to deposit the films. Transmission measurements were performed using Perkin-Elmer Lambda 750 spectrometer.

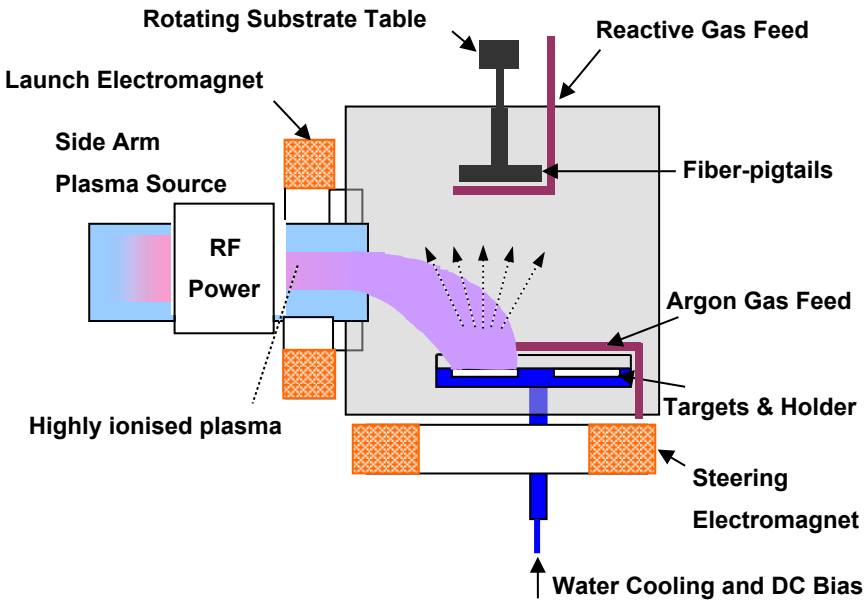

Figure S7 | The remote plasma sputtering deposition schematic drawing.

References

S1. Li, H., Zhang, Q., Yap, C. C. R., Tay, B. K., Edwin, T. H. T., Olivier, A., & Baillargeat, D. From bulk to monolayer MoS_2: evolution of Raman scattering. *Adv. Funct. Mater.*, **22**, 1385-1390 (2012).

S2. Radisavljevic, B., Radenovic, A., Brivio, J., Giacometti, V. & Kis, A. Single-layer MoS_2 transistors. *Nat. Nanotech.* **6**, 147-150 (2011).

S3. Wilson, J. A., & Yoffe, A. D.. The transition metal dichalcogenides discussion and interpretation of the observed optical, electrical and structural properties. *Adv. Phys*. **18**, 193-335 (1969)

S4. Wang, X., Gong, Y., Shi, G., Chow, W. L., Keyshar, K., Ye, G., ... & Ajayan, P. M.. Chemical vapor deposition growth of crystalline monolayer $MoSe_2$. *ACS nano*, 8(5), 5125-5131 (2014).

S5. Yun, W. S., Han, S. W., Hong, S. C., Kim, I. G. & Lee, J.D. Thickness and strain effects on electronic structures of transition metal dichalcogenides: 2H-M X-2 semiconductors (M = Mo, W; X = S, Se, Te). *Phys Rev B* **85**, 033305 (2012).